Effect of natural convection on oscillating flow in a pipe with cryogenic temperature difference across the ends

T.R. Ashwin[a], **G.S.V.L. Narasimham**[a,*], **Subhash Jacob**[b]

[a]**Department of Mechanical Engineering**

[b]**Centre for Cryogenic Technology**

Indian Institute of Science, Bangalore 560012, India

Abbreviated Title: Buoyancy effect on oscillating flow

Abstract: The effect of natural convection on the oscillatory flow in an open-ended pipe driven by a timewise sinusoidally varying pressure at one end and subjected to an ambient-to-cryogenic temperature difference across the ends, is numerically studied. Conjugate effects arising out of the interaction of oscillatory flow with heat conduction in the pipe wall are taken into account by considering a finite thickness wall with an insulated exterior surface. Two cases, namely, one with natural convection acting downwards and the other, with natural convection acting upwards, are considered. The full set of compressible flow equations with axis-symmetry are solved using a pressure correction algorithm. Parametric studies are conducted with frequencies in the range 5-15 Hz for an end-to-end temperature difference of 200 K and 50 K. Results are obtained for the variation of velocity, temperature, Nusselt number and the phase relationship between mass flow rate and temperature. It is found that the Rayleigh number has a minimal effect on the time averaged Nusselt number and phase angle. However, it does influence the local variation of velocity and Nusselt number over one cycle. The natural convection and pressure amplitude have influence on the energy flow through the gas and solid.

Keywords: Pulse tube, Natural convection, Conjugate conduction.

∗:Corresponding author. Telephone: +91-80-22932971, Fax: +91-80-23600648

Email address: mecgsvln@mecheng.iisc.ernet.in (Narasimham, G.S.V.L)

Nomenclature

c_p	constant pressure specific heat	$(\mathrm{J\,kg^{-1}\,K^{-1}})$
D,d	diameter	(m)
$\dot{E}$	enthalpy flow	(W)
Ec	Eckert number, $v_\mathrm{c}^2/c_{\mathrm{p,c}}\,T_\mathrm{c}$	dimensionless
f	frequency	(Hz)
Gr	Grashof number $g\epsilon L_c^3/\nu_c^2$	dimensionless
g	acceleration due to gravity	$(\mathrm{m\,s^{-2}})$
H	length of tube	(m)
h	heat transfer coefficient	$(\mathrm{W\,m^{-2}\,K^{-1}})$
k	thermal conductivity	$(\mathrm{W\,m^{-1}\,K^{-1}})$
L	length	m
$\dot{M}$	mass flow rate	$\mathrm{kg\,s^{-1}}$
Nu	Nusselt number, $h\,R_\mathrm{i}/k$	dimensionless
p	pressure	(Pa)
Pr	Prandtl number, $\mu\,c_\mathrm{p}/k$	dimensionless
R	radius	(m)
Ra	Rayleigh number $g\epsilon L_c^3/\nu\alpha$	dimensionless
Re	Reynolds number, $\omega R_\mathrm{i}^2\,\rho/\mu$	dimensionless
T	temperature	(K)
t	time	(s)
v	velocity	$(\mathrm{m\,s^{-1}})$

Greek Symbols

ΔT_c	characteristic temperature difference	K
γ	ratio of specific heats	dimensionless
α	thermal diffusivity	m^2/s
ϵ	overheat ratio	dimensionless
μ	dynamic viscosity	$(kg\,m^{-1}\,s^{-1})$
ν	kinematic viscosity	$(m^2\,s^{-1})$
ρ	density	$(kg\,m^{-3})$
ω	angular frequency	$(rad\,s^{-1})$

Subscripts

a	amplitude
av	average
c	characteristic
e	evaporator or cold
f	fluid region
h	hot or ambient
i	inner
o	outer, charge pressure
p	time period
r	radial direction
s	solid region
w	wall
z	axial direction

Superscript

*	dimensionless quantity

1 Introduction

Oscillating flow problems have practical applications in equipment like Stirling engines and refrigerators, regenerators, combustor pipes, pulse tube coolers, pipe manifolds and in biological systems in relation to blood flow. The effect of natural convection on the oscillating flow is important in devices like pulse tubes with a cold heat exchanger of cryogenic temperature at one end and ambient hot heat exchanger at the other end. Oscillating flow problems in pipes have received relatively less attention. Buoyancy effect in oscillating flows has received even less attention. The work reported in the area of natural convection in pipes is mostly confined to through flow produced by buoyancy in vertical and inclined pipes. A few studies have considered pipes with closed ends. The present authors have earlier considered the problem of oscillating flow and heat transfer in an open tube with negligible buoyancy forces [1]. Hence the results reported are applicable to a horizontal pipe or for situations with negligible gravity. However, for vertical geometries, the effect of buoyancy becomes important, which is the subject of the present study. The study is performed with low pressure amplitudes with buoyancy acting upward and downward to differentiate the effect of natural convection in oscillating flows.

Natural convection in a vertical cylinder with adiabatic lateral walls with constant but different temperatures on the end surfaces has been studied numerically by He et al. [2]. The results extend the chart of Catton and Edward for L/D ratios 2.5-10. In the case of large temperature difference ($\Delta T = 200$ K), the natural convection in the enclosure is quite strong in that the convective heat transfer rate is about two orders larger than that of pure heat conduction. This occurs when the cold end is placed down. The investigators have suggested to arrange the pulse tube with the cold end at the bottom position. Other contributions relevant to oscillating flows are Al-Haddad and Al-Binally [3], Cho and Hyun [4], Faghri et al. [5], Moschandreou and Zamir [6], Guo and Sung [7] and Chattopadhyay et al. [8]. These are already covered in Ashwin et al. [1].

2 Formulation

2.1 Geometry

Fig. 1 shows the physical model and coordinate system. Cylindrical polar coordinate system is chosen with the assumption of axisymmetric flow and temperature distributions. The model consists of a cylindrical pipe open at both ends, with a finite wall thickness. Two configurations are studied. In the first one the gravity vector is parallel to the z-axis and acts vertically downwards (i.e. the angle between gravity vector and z-axis is 180°). The other one is an inverted configuration with the gravity vector acting vertically upwards (i.e. the angle between the gravity vector and z-axis is 0°). The working medium at the ends of the tube is assumed to be isothermal but at different temperatures. For example, these regions correspond to the cold and warm heat exchangers of a pulse tube refrigerator. The working medium when entering one of the ends does so at a cryogenic temperature T_{e}, while the working medium entering the other end of the tube is at a higher temperature T_{h} (typically room temperature). The oscillating flow in the tube is driven by a sinusoidally varying pressure at the cold end of the tube. Since the so called DC component is absent, the fluid flow during a cycle takes place partly into and partly out of the tube at either end. The height of the tube and the inner and outer radii are H, R_{i} and R_{o}, respectively. Clearly the wall thickness δ_{w} is $R_{\mathrm{o}} - R_{\mathrm{i}}$. The oscillating heat transfer between the wall and the gas is taken into account through the coupling between the fluid and the solid at the interface. The annular surfaces of the solid at the tube ends are assumed to be insulated.

2.2 Non-dimensionalisation

The characteristic length L_{c} is taken as the inner radius R_{i} of the tube and the characteristic temperature T_{c} as the hot heat exchanger temperature T_{h}, which is also the ambient temperature. The geometrical parameters of the problem are the dimensionless inner radius R_{i}^* of the tube, dimensionless height H^* and the dimensionless wall thickness δ_{w}^*. The characteristic density ρ_{c} corresponds to the state of helium at the charge pressure p_{o} and ambient temperature $T_{\mathrm{h}} = T_{\mathrm{c}}$. The characteristic thermal conductivity, specific heat and dynamic viscosity of the working medium, i.e. helium gas, correspond to T_{c} and are denoted respectively k_{c}, $c_{\mathrm{p,c}}$ and μ_{c}. The dimensionless temperature T^* is $(T - T_{\mathrm{c}})/\Delta T_{\mathrm{c}}$ where ΔT_{c} is $T_{\mathrm{h}} - T_{\mathrm{e}}$. The

quantity $\epsilon = \Delta T_\mathrm{c}/T_\mathrm{c}$ is the overheat ratio. The characteristic pressure is p_c is taken as $\rho_\mathrm{c} v_\mathrm{c}^2$ where v_c, the characteristic velocity, is taken as ωL_c, the quantity ω being the angular frequency. The time is non-dimensionalised with the time period of the oscillation $1/\omega$. Thus the dimensionless time period t_p^* is 2π.

The dimensionless quantities are defined as:

$$
\begin{aligned}
&t^* = t\omega,\ r^* = \frac{r}{L_\mathrm{c}},\ z^* = \frac{z}{L_\mathrm{c}},\ L_\mathrm{c} = R_\mathrm{i} \\
&v_\mathrm{r}^* = \frac{v_\mathrm{r}}{v_\mathrm{c}},\ v_\mathrm{z}^* = \frac{v_\mathrm{z}}{v_\mathrm{c}},\ p^* = \frac{p}{\rho_\mathrm{c} v_\mathrm{c}^2},\ v_\mathrm{c} = \omega L_\mathrm{c} \\
&T^* = \frac{T - T_\mathrm{c}}{\Delta T_\mathrm{c}},\ \epsilon = \frac{\Delta T_\mathrm{c}}{T_\mathrm{c}},\ \Delta T_\mathrm{c} = T_\mathrm{h} - T_\mathrm{e},\ T_\mathrm{c} = T_\mathrm{h} \\
&\rho^* = \frac{\rho}{\rho_\mathrm{c}},\ c_\mathrm{p}^* = \frac{c_\mathrm{p}}{c_\mathrm{p,c}},\ \mu^* = \frac{\mu}{\mu_\mathrm{c}},\ k^* = \frac{k}{k_\mathrm{c}} \\
&Re = \frac{v_\mathrm{c} L_\mathrm{c} \rho_\mathrm{c}}{\mu_\mathrm{c}},\ Pr = \frac{\mu_\mathrm{c} c_\mathrm{p,c}}{k_\mathrm{c}},\ Ec = \frac{v_\mathrm{c}^2}{c_\mathrm{p,c} T_\mathrm{c}},\ Gr_c = \frac{g\epsilon L_c^3}{\nu_c^2} \\
&H^* = \frac{H}{L_\mathrm{c}},\ \delta_\mathrm{w}^* = \frac{\delta_\mathrm{w}}{L_\mathrm{c}}
\end{aligned}
$$

The dimensionless outer radius is $R_\mathrm{o}^* = R_\mathrm{o}/L_\mathrm{c} = (R_\mathrm{i} + \delta_\mathrm{w})/L_\mathrm{c} = R_\mathrm{i}^* + \delta_\mathrm{w}^* = 1 + \delta_\mathrm{w}^*$ (since $R_\mathrm{i}^* = 1$) and the dimensionless charge pressure $p_\mathrm{o}^* = p_\mathrm{o}/(\rho_\mathrm{c} v_\mathrm{c}^2)$. The dimensionless properties should correspond to the fluid or solid depending upon the region under consideration, i.e. the working medium or wall. Thus the dimensionless ratios, namely, μ_f^*, $c_\mathrm{p,f}^*$ and k_f^*, the subscript 'f' denoting fluid, are assigned a value of unity in the fluid domain. In the solid region, the property values should correspond to those of the solid, namely, k_s^* and $c_\mathrm{s}^* = c_\mathrm{s}/c_\mathrm{p,c}$. In the numerical analysis, the solid is treated as a fluid of infinite viscosity.

2.3 Dimensionless governing equations

The dimensionless continuity, momentum and energy equations are as follows:

Continuity equation

$$\frac{\partial \rho^*}{\partial t^*} + \frac{1}{r^*}\frac{\partial}{\partial r^*}(r^* \rho^* v_\mathrm{r}^*) + \frac{\partial}{\partial z^*}(\rho^* v_\mathrm{z}^*) = 0 \tag{1}$$

Momentum equation in the radial direction

$$\frac{\partial}{\partial t^*}(\rho^* v_{\mathrm{r}}^*) + \frac{1}{r^*}\frac{\partial}{\partial r^*}(r^*\rho^* v_{\mathrm{r}}^* v_{\mathrm{r}}^*) + \frac{\partial}{\partial z}(\rho^* v_{\mathrm{z}}^* v_{\mathrm{r}}^*) = -\frac{\partial p^*}{\partial r^*} + \frac{1}{Re}\left[\frac{1}{r^*}\frac{\partial}{\partial r^*}\left(r^*\mu^*\frac{\partial v_{\mathrm{r}}^*}{\partial r^*}\right)\right.$$
$$\left. + \frac{\partial}{\partial z^*}\left(\mu_*\frac{\partial v_{\mathrm{r}}^*}{\partial z^*}\right)\right] + S_{\mathrm{r}} \tag{2}$$

Momentum equation in axial direction

$$\frac{\partial}{\partial t^*}(\rho^* v_{\mathrm{z}}^*) + \frac{1}{r^*}\frac{\partial}{\partial r^*}(r^*\rho^* v_{\mathrm{r}}^* v_{\mathrm{z}}^*) + \frac{\partial}{\partial z^*}(r^*\rho^* v_{\mathrm{z}}^* v_{\mathrm{z}}^*) = -\frac{\partial p^*}{\partial z^*} + \frac{1}{Re}\left[\frac{1}{r^*}\frac{\partial}{\partial r^*}\left(r^*\mu^*\frac{\partial v_{\mathrm{z}}^*}{\partial r^*}\right)\right.$$
$$\left. + \frac{\partial}{\partial z^*}\left(\mu^*\frac{\partial v_{\mathrm{z}}^*}{\partial z^*}\right)\right] + S_{\mathrm{z}} \tag{3}$$

Energy equation

$$\frac{\partial}{\partial t^*}(\rho^* T^*) + \frac{1}{r^*}\frac{\partial}{\partial r^*}(\rho^* r^* v_{\mathrm{r}}^* T^*) + \frac{\partial}{\partial z^*}(\rho^* v_z^* T^*) = \frac{1}{RePr}\left[\frac{1}{r^*}\frac{\partial}{\partial r^*}\left(\frac{k^*}{c_{\mathrm{p}}^*}r^*\frac{\partial T^*}{\partial r^*}\right)\right.$$
$$\left. + \frac{\partial}{\partial z^*}\left(\frac{k^*}{c_{\mathrm{p}}^*}\frac{\partial T^*}{\partial z^*}\right)\right] + \frac{Ec}{c_{\mathrm{p}}^*\,\epsilon}\frac{Dp^*}{Dt^*} \tag{4}$$

Equation of state

$$p^* = \frac{1}{Ec}\,\rho^*\,\frac{\gamma - 1}{\gamma}(T^*\,\epsilon + 1) \tag{5}$$

The momentum source terms are given by:

$$S_{\mathrm{r}} \quad = \frac{1}{Re}\left[\frac{\partial}{\partial z^*}\left(\mu^*\frac{\partial v_{\mathrm{z}}^*}{\partial r^*}\right) + \frac{1}{r^*}\frac{\partial}{\partial r^*}\left(r^*\mu^*\frac{\partial v_{\mathrm{r}}^*}{\partial r^*}\right) - \frac{2\mu^* v_{\mathrm{r}}^*}{r^{*2}} - \frac{2}{3}\frac{\partial}{\partial r^*}\left(\mu^* D^*\right)\right] \tag{6}$$
$$+\frac{Gr_c}{{Re_{R,c}}^2}\frac{1}{\epsilon}((\rho^* - 1)\vec{g} \bullet \vec{e_r})$$

$$S_{\mathrm{z}} \quad = \frac{1}{Re}\left[\frac{\partial}{\partial z^*}\left(\mu_*\frac{\partial v_{\mathrm{z}}^*}{\partial z^*}\right) + \frac{1}{r^*}\frac{\partial}{\partial r^*}\left(r^*\mu^*\frac{\partial v_{\mathrm{r}}^*}{\partial z^*}\right) - \frac{2}{3}\frac{\partial}{\partial r^*}(\mu^* D^*)\right] \tag{7}$$
$$+\frac{Gr_c}{{Re_c}^2}\frac{1}{\epsilon}((\rho^* - 1)\vec{g} \bullet \vec{e_z})$$

where the dimensionless divergence is given by:

$$D^* = \frac{1}{r^*}\frac{\partial}{\partial r^*}(r^* v_{\mathrm{r}}^*) + \frac{\partial v_{\mathrm{z}}^*}{\partial z^*}$$

The substantive derivative Dp^*/Dt^* is given by:

$$\frac{Dp^*}{Dt^*} = \frac{\partial p^*}{\partial t^*} + v_{\mathrm{r}}^*\frac{\partial p^*}{\partial r^*} + v_{\mathrm{z}}^*\frac{\partial p^*}{\partial z^*}$$

2.4 Nusselt number and enthalpy flow

The Nusselt number at any axial location on the fluid-solid interface and at any time is defined as

$$Nu_{\mathrm{z,t}} = \left[\frac{\partial T^*}{\partial r^*}\right]_{r^*=R_{\mathrm{i}}^*} \tag{8}$$

The Nusselt number Nu_{av} is the average of Nu_{z} over the length of the interface and one time period.

$$Nu_{\mathrm{av}} = \frac{1}{H^*\, t_{\mathrm{p}}^*} \int_0^{H^*} \int_0^{t_{\mathrm{p}}^*} Nu_{\mathrm{z,t}}\, dz\, dt \tag{9}$$

The enthalpy flow through any cross-section is calculated as:

$$\dot{E}_{\mathrm{av}} = \frac{1}{\pi\, R_{\mathrm{i}}^{*2}} \int_0^{R_{\mathrm{i}}^*} \rho^*\, v_z^* c_p^* T^* (2\pi\, r^* dr^*) \tag{10}$$

The pressure oscillation at the inlet of the pipe is:

$$p^*(t^*) = p_{\mathrm{o}}^* + p_{\mathrm{a}}^* \sin(t^*) \tag{11}$$

where p_o^* is the dimensionless charge pressure.

2.5 Initial and boundary conditions

It is assumed that at the beginning (i.e. $t^* = 0$), the geometry is under ambient condition and the system is filled with helium gas at the charge pressure. These conditions are taken as 300 K and 25 bar.

No-slip and zero mass permeability is assumed on the solid boundary in contact with the fluid. Oscillating pressure and zero radial velocity are prescribed at the cold end of the tube. At the hot end of the tube, zero streamwise derivative of the radial velocity is prescribed. The axial velocities at the inlet and outlet are calculated using the continuity equation. On the axis of the tube, zero cross-stream derivative of the axial velocity and zero radial velocity are imposed.

At the interface between the solid and the fluid, heat flux continuity and no temperature jump conditions should be satisfied. This is done through the harmonic mean thermal conductivity method [9]. At the cold end, the temperature condition is taken as the cold heat exchanger temperature when the flow takes place into the tube and as zero axial temperature gradient when the flow is out of the tube. Similar conditions are also applied at the hot end of the tube.

2.6 Dimensionless initial and boundary conditions

The initial and boundary conditions mentioned earlier, take the following form upon non-dimensionalization.

At $t^* \leq 0$: $v_{\mathrm{r}}^* = v_{\mathrm{z}}^* = 0$, $T^* = 1$ and $p^* = p_{\mathrm{c}}/(\rho_{\mathrm{c}} v_{\mathrm{c}}^2)$ ($0 \leq r \leq R_o$ and $0 \leq z \leq H$). The quantity v_{c} is given by ωL_{c}.

$$\begin{aligned} &v_{\mathrm{r}}^*(0, z^*, t^*) = 0;\ v_{\mathrm{r}}^*(1, z^*, t^*) = 0;\ v_{\mathrm{r}}^*(r^*, 0, t^*) = 0; \\ &\frac{\partial v_{\mathrm{r}}^*}{\partial z^*}(r^*, H^*, t^*) = 0;\ \frac{\partial v_{\mathrm{z}}^*}{\partial r}(0, z^*, t^*) = 0 \end{aligned} \tag{12}$$

The last relation states that the radial derivative of axial velocity is zero on the axis in view of the symmetry.

$$\begin{aligned} &\text{If } v_{\mathrm{z}}^*(r^*, 0, t^*) \leq 0 \text{ then } \frac{\partial T^*}{\partial z^*}(r^*, 0, t^*) = 0 \\ &\text{If } v_{\mathrm{z}}^*(r^*, 0, t^*) > 0 \text{ then } T^*(r^*, 0, t^*) = -1.0 \\ &\text{If } v_{\mathrm{z}}^*(r^*, H^*, t^*) > 0 \text{ then } \frac{\partial T^*}{\partial z^*}(r^*, H^*, t^*) = 0 \\ &\text{If } v_{\mathrm{z}}^*(r^*, H^*, t^*) \leq 0 \text{ then } T^*(r^*, H^*, t^*) = 1.0 \end{aligned} \tag{13}$$

At the interface:

$$-k_{\mathrm{f}}^* \frac{\partial T_{\mathrm{f}}^*}{\partial r^*} = -k_{\mathrm{s}}^* \frac{\partial T_{\mathrm{s}}^*}{\partial r^*};\ T_{\mathrm{f}}^* = T_{\mathrm{s}}^* \text{ at } r = R_{\mathrm{i}} \tag{14}$$

The driving parameters of the problem are Ec, Re, Pr and ϵ.

3 Parametric Studies

The numerical method, grid dependency study and validation of the computer code are reported in an earlier paper [1]. Results are obtained for tube of length of 100 mm and diameter

8 mm (i.e. the length-to-diameter ratio is 12.5). Two end temperature differences, 200 K and 50 K, are tested, keeping the hot end at a constant value of 300 K and choosing the cold end temperature as 250 K and 100 K. The corresponding Rayleigh number based on the pipe diameter ranges from 4.87×10^6 for 200 K temperature difference and 1.22×10^6 for 50 K. The frequency ranges from 5 to 15 Hz. As mentioned in section 2.1, two cases, one with hot end at the top and the other with cold end at the top are studied. The details of the parametric studies are given in Table 1. The full compressible system of equations is solved, without invoking the Boussinésq assumption. The problem is computation-intensive with each run taking more than 7 days of continuous running on a SUN workstation of 64-bit architecture with 15 GB RAM. Inclusion of variable transport properties (viscosity and thermal conductivity) results in even larger computing times. However, there is only a small deviation between the constant and variable transport property results (0.22% in temperature and 0.9% in velocity). Hence most of the results presented are obtained with constant transport properties.

4 Results and Discussion

4.1 The effect of orientation on temperature profiles

Figs. 2(a) and 2(b) show the temperature contours inside the tube after attaining steady periodic condition with hot end at the top for the higher Rayleigh number. The pressure amplitude is 50 Pa. The isotherms in the profiles are smooth and vertical to the wall and the axis in the major part of the tube. They are very crowded near the cold end where sharp temperature gradients exist. The hot end and the middle cross section of the tube show more uniform temperature compared to the region near the cold end. The outer wall of the tube is kept at adiabatic condition. But there is always heat transfer between solid and the wall inside the tube. Figs. 2(c) and 2(d) show the temperature profiles with hot end at the bottom. It can be seen that the smoothness in the isotherms is completely lost and there is considerable distortion in the profiles due to the influence of natural convection occurring in the tube due to the placement of hot end at the lower side. Thus this configuration tends to destroy the temperature gradient in the tube, making the temperature in the middle portion more or less uniform. There is an upward flow of gas due to the positioning of hot end downwards. Near the wall, the isotherms are still smooth and vertical. The results show that the positioning of hot

and cold heat exchangers is important in pulse tube refrigerators. The general conclusion is that for any type of open tubes with similar configuration, three main zones can be identified. The cold gas zone near the cold end, a hot gas zone near the hot end and a central buffer zone separating the above mentioned zones. Placing the hot heat exchanger at the bottom will smear the temperature gradient in the tube and will result in mixing of gases inside the tube which will decease the efficiency.

Fig. 3 shows similar set of results for the lower Rayleigh number. The profiles are almost similar to Fig. 2. The profiles at frequencies of 5 Hz and 10 Hz also look almost similar for both the Rayleigh numbers.

Fig. 4 shows the variation of cross-sectionally averaged axial velocity and temperature for 5 Hz frequency for 50 Pa pressure amplitude after attaining steady periodic condition for $Ra = 4.9 \times 10^6$ at the middle cross-section of the tube. The temperature profiles in Fig. 4(a) show a temperature oscillation between 296.5 K and 296.2 K when the hot end is at the top. With cold end at the top, the temperature oscillates between 299.9 K and 299.69 K. Clearly this behavior in the temperature oscillation is due to the influence of natural convection. Cold end temperature is found to be diffusing more into the middle section for first configuration and hot end temperature is more diffusing for the second configuration. This is due to the fact that the configuration with hot end down will aid the natural convection effect and keeps the middle cross section nearer to hot end temperature. It is conjectured that at higher pressure amplitudes, the periodic flow effect suppresses the natural convection effect. The velocity profiles are shown in Fig. 4(b) for both the configurations. For hot side up configuration, the velocities are oscillating in positive and negative directions. Thus for hot end at top configuration, the velocity is experiencing oscillation. But for hot end bottom configuration, the buoyancy overpowers the oscillatory flow producing a unidirectional flow.

4.2 The effect of pressure amplitude on temperature profiles

Fig. 5 shows the cross-section averaged temperature profiles at different cross-sections, namely, $0.25H$, $0.5H$ and $0.75H$, inside the tube. The results are for 15 Hz and $Ra = 1.22 \times 10^6$ with hot end at the top. Figure 6 is for the case of hot end at the bottom. The variation of the temperature is shown for one time period.

Fig. 5(a) shows that the temperature settles at 299.1 K at $0.25H$ and 299.9 K at $0.75H$

for 50 Pa pressure amplitude. Fig. 5(b) shows that the temperature settles at 290 K at $0.25H$ and 298 K for $0.75H$ for 500 Pa pressure amplitude. The temperatures for $0.5H$ and $0.75H$ are found to be almost the same for both the cases. Thus as the pressure amplitude increases, a strong axial temperature gradient is established in the solid tube wall.

Comparing Figs. 5 and 6, it can be seen that at lower pressure amplitudes, the temperature profile is not getting distorted much. But for the case of higher pressure amplitude, there is an appreciable distortion in the profile. Also there is sharp dip in the temperature profile near the entry. This deviation can be due to the inertial effect of the higher density fluid near the cold end. Comparing Figs. 5(b) and 6(b), the distortion in configuration with hot end down is even more, due to the effect of natural convection.

4.3 Variation in axial temperature profiles

Fig. 7 shows the temperature variations in the solid and the gas for 5 Hz frequency with hot end up and down configurations for 50 Pa of inlet driving pressure amplitude for two Rayleigh numbers. The temperatures are plotted at a particular instant of operation after attaining steady periodic condition.

From Figs. 7(a) and 7(b), it can be observed that for the higher Rayleigh number case, the cold and hot end solid temperatures are 221 K and 299 K for the hot end up case, and 229 K and 299 K for the hot end down case. The zero distance refers to the cold end. There is a sharp temperature rise in the solid near the cold heat exchanger. Also the temperature difference between the solid and the fluid becomes higher as the cold is approached. Figs. 7(c) and 7(d) show the axial temperature distribution for the lower Rayleigh number. It may be noted that the end-to-end temperature difference is more pronounced in the case of lower Rayleigh number. The solid temperature stabilizes at 266 K in the hot end up case and at 284 K in the hot end down case, 299 K being the hot end temperature for both the cases. From these results, it appears that reversing the orientation of the tube such that hot end is at the bottom tends to rise the temperature at the cold end substantially. The shape of the solid temperature profile is non-linear due to the solid-gas heat exchange.

Although not shown here, the solid-to-gas temperature difference for 500 Pa pressure amplitude for high Rayleigh number with hot side up case is observed to be as low as 2 K at the cold end. The same is much higher for the lower pressure amplitude as can be seen

from Fig. 7(a). This behavior is traced to the mixing of gas inside the tube. There is higher chance for mixing at the inlet region at higher pressure amplitudes, leading to equalization of the gas-solid temperature. Thus high pressure amplitudes usually pump more heat into the solid wall of the tube. From the heat balance presented later, it can be seen that there is a decrease in the overall axial solid temperature gradient for configurations with hot end down.

4.4 Comparison of constant and variable transport property results

A comparison of the constant and variable transport property results for the temperature and velocity variation at the middle cross section of the tube with a pressure amplitude of 50 Pa with hot side up is shown in Fig. 8, the Rayleigh number being 1.22×10^6. The results correspond to a time of 501 seconds, by which a steady periodic condition has already been attained. The temperature dependence of the viscosity and thermal conductivity of helium is taken from Touloukian and Liley [10] and the variable properties of Stainless steel are taken form NIST database [11]. It is observed that the maximum deviation caused with constant properties in temperature and velocity are 0.22% (Fig. 8(a)) and 0.9% (Fig. 8(b)), respectively.

4.5 Heat transfer between wall and gas

Fig. 9 shows the heat transfer between gas and the wall at different points inside the tube at the higher Rayleigh number for hot end up and down configurations for a frequency of 10 Hz and 50 Pa pressure amplitude. The axial locations on the interface are at $0.25H$, $0.5H$ and $0.75H$.

The positive heat flux indicates that the heat transfer is from the solid to the gas. Figs. 9(a) and 9(b) show that at some instances in a cycle there is flow of heat from gas to wall (negative flux) and at some instances it is form solid to gas. This heat transfer from and to the wall differs from point to point for different cases as the distance increases from cold end to hot end. It should be noted that the specific heat ratio of solid to gas is very large. The thermal inertia of the solid attenuates the oscillatory nature of the temperature during startup and after attaining periodic condition. The heat fluxes at $0.5H$ and $0.75H$ almost coincide and therefore cannot be distinguished due to overlapping. This gives the conclusion that the time variation of the heat flux is almost the same for all locations in the range $0.5H$-H.

4.6 Velocity and Nusselt number variations

Fig. 10 shows the area-averaged axial velocity variation inside the tube for 500 Pa pressure amplitude at 15 Hz for $Ra = 1.22 \times 10^6$ at the cold end. Fig. 11 shows the corresponding Nusselt number variation. The results correspond to times of 6.66, 100.33 and 167 seconds after the startup. From Figs. 10(a) and 10(b), the velocity is seen to have positive and negative parts in a cycle in the beginning, for instance, after 6.66 seconds. This means that the gas inside the tube oscillates (i.e. moves in both directions) and experiences a complete flow reversal in the beginning. At a time of 100.33 and 167 the positive portion decreases and negative contribution increases. This is due to the change in density due to cooldown and also the effect of natural convection acting on the tube. There is a diffusion of cold end temperature into the tube and the density inside the tube changes rapidly. Velocity profiles in the cases with hot end down (Fig. 10(b)) have only negative flow after attaining steady periodic condition but the oscillating nature persists.

The behavior trend in the velocity profiles can be explained as follows. Assuming that there is a constant part and variable part for the velocity oscillation, the variable part is due to the sinusoidal driving force at the inlet of the tube and the constant part is due to the effect of natural convection. Since this is an open tube, natural convection will occur either upwards or downwards depending on the temperature difference. The variable part of velocity will experience changes due to the variation in density. The constant part or unidirectional part, due to the influence of natural convection, is mainly controlled by change in density changes inside the tube (or Rayleigh number), orientation and boundary conditions. The balance of the two effects determines the oscillating nature of gas inside the tube. In the the first case (Fig. 10(a)) the velocity variation is controlled mainly by the pressure oscillation at inlet and in the second case (Fig. 10(b)), by the effect of natural convection. The dominance of negative velocity in Fig. 10(b) is due to the pushing of gas downwards due to the very low cold end temperature (and hence higher density) compared to the hot end.

Fig. 11 shows the variation of Nusselt number over one cycle with hot end facing up as well as down. It can be seen that the average Nusselt number variation is not affected much by the orientation and that it becomes smoother as more time elapses from the startup. The value of Nusselt number increases and decreases during a cycle, positive Nusselt number indicating heat transfer from wall to gas. The variation in the Nusselt number follows the same pattern as that of the average velocity over one cycle. Although there is gas-to-solid surface

heat pumping in the tube, this quantity will be small compared to pressure heat pumping (i.e. enthalpy flow). However, surface heat pumping can become significant in high frequency pulse tube refrigerators.

Table 2 shows the time averaged Nusselt number at the solid-gas interface for all the cases. The average Nusselt number is based on the end-to-end temperature difference 9. The values of the average Nusselt number are rather low compared to incompressible flow [8] and do not change much with frequency of operation, pressure amplitude, orientation or end temperature difference. The Nusselt number can be used for finding the heat transfer between gas and the wall over one cycle.

4.7 Energy balance for various models

Tables 3 and 4 show the energy balance for different models, at the higher and lower Rayleigh numbers, with hot end facing upwards and downwards. It can be observed from these tables that the energy flow through gas as well as solid at $0.5\,H$ and $0.75\,H$ remains constant. Also the energy flow through the wall is very minimal compared to the energy flow through the gas.

It can be observed from the above tables that the energy flow through the solid and the gas increases with increase in pressure amplitude. Increase in pressure amplitude increases the velocity and mass flow rate, promoting the enthalpy flow through the gas. Also the increase in velocity magnitude due to higher pressure amplitude enhances the mixing of gases leading to a decrease in the thermal resistance near the solid-fluid interface. This phenomenon pumps more heat into the solid from gas. It can be seen from Table 3 that the solid energy flow increases with pressure amplitude. However, for the hot end down configuration, there is an additional effect from natural convection.

From the heat transfer data, it can be seen that at low pressure amplitude, the frequency of oscillation has a negligible effect on the energy transfer through the solid. But it has some effect for higher frequencies and higher pressure amplitudes.

For cases with hot end placed down, there is a marginal increases in the energy transfer through the solid and the gas. This is due to the influence of natural convection aiding the flow. Since in devices like pulse tubes, higher axial conduction through solid is not desirable, the configuration in which hot end is placed at the top gives better performance due to lower

axial conduction.

4.8 Phase relationships

Fig. 12 shows the phase relationship between the temperature and mass flow rate at the middle cross-section of the tube after periodic condition is achieved for frequency of 5 Hz with 50 Pa pressure amplitude. These are the area-averaged quantities over the cross-section. The heat absorbed or released depends upon the phase relationship between the mass flow and the temperature, and this is important for designing devices like pulse tube refrigerator. Assuming ideal gas relation, the enthalpy flow over a cycle can be written as:

$$\dot{E} = \frac{1}{t_{\mathrm{p}}} \oint_0^{t_{\mathrm{p}}} \dot{M} c_{\mathrm{p}} dt \tag{15}$$

It can be seen from Fig. 12 that temperature leads the mass flow rate for both the frequencies. The phase relationship between these quantities depends upon several factors like geometrical dimensions of the tube, the frequency and the pressure amplitude. Ideally the temperature should be in phase with the mass flow rate for maximum enthalpy flow rate. From figures 12(a) and 12(b), the phase angle remains almost same for both the configurations. For the first case, peak to peak difference is approximately 0.051 seconds and for the second case it is 0.058 seconds. Figure 12(c) shows the values at lower Rayleigh number, the difference is approximately 0.056 seconds. Thus the effect of orientation and temperature difference across the ends on phase angle is minimum for the geometry and boundary conditions selected.

5 Conclusions

The problem of conjugate natural convection in an oscillating flow pipe with finite wall thickness and temperature difference across the ends is studied for frequencies of 5-15 Hz temperature difference of 50 K and 200 K. The distortion in isothermal lines are found to be more when hot end is placed down. It is therefore advisable to keep the hot end up for better functioning of devices like pulse tube coolers wherein this kind of conditions are encountered. The hot end temperature is to found diffuse more into the tube when the hot end is down. Also the gas velocity profiles inside the tube are affected by the natural convection inside the

tube. At higher pressure amplitudes there is a sharp dip in the temperature profiles near the entry. This can be due to the inertial effects of the gas. Natural convection amplifies this distortion. Also higher pressure amplitude is capable of producing sharp temperature gradient in the solid. This is due to more intense gas-solid interaction at the interface at higher amplitudes. The time averaged Nusselt number does not change significantly with orientation or Rayleigh number. Natural convection results in a complex variation of the Nusselt number and velocity in a cycle compared to the case where buoyancy is negligible. An increase in the energy transfer through solid as well as gas is observed for cases with hot end placed down. The Rayleigh number does not have much effect on heat flow through the gas and solid at lower pressure amplitudes.

References

[1] T.R. Ashwin, G.S.V.L. Narasimham, S. Jacob, Oscillatory flow and temperature fields in an open tube with temperature difference across the ends, International Journal of Heat and Mass Transfer 54 (2011) 3357-3368.

[2] Y.L. He, W.Q. Tao, Z.G. Qu, Z.Q. Chen, Steady natural convection in a vertical cylindrical envelope with adiabatic lateral wall, International Journal of Heat and Mass Transfer, 47 (2004) 3131-3144.

[3] A.A. Al-Haddad, N. Al-Binally, Prediction of heat transfer coefficient in pulsating flow, International Journal of Heat and Fluid Flow 10 (1989) 131-133.

[4] H.W. Cho, J.M. Hyun, Numerical solutions of pulsating flow and heat transfer characterestics in a pipe, International Journal of Heat and Fluid Flow 11 (1990) 321-330.

[5] M. Faghri, K. Javdani, A. Faghri, Heat transfer with laminar pulsating flow in a pipe, Letters in Heat and Mass Transfer, 6 (1979) 259-270.

[6] T. Moschandreou, M. Zamir, Heat transfer in a tube with pulsating flow and constant heat flux, International Journal of Heat Mass Transfer, 40 (1997) 2461-2466.

[7] Z. Guo, H.J. Sung, Analysis of the Nusselt number in pulsating pipe flow, International Journal of Heat and Mass Transfer 40 (1997) 2486-2489.

[8] H. Chattopadhyay, F. Durst, S. Ray, Analysis of heat transfer in simultaneously developing pulsating laminar flow in a pipe with constant wall temperature, International Communications in Heat and Mass Transfer 33 (2006) 475-481.

[9] S.V. Patankar, Numerical heat transfer and fluid flow, in: W.J. Minkowycz, E.M. Sparrow (Eds.), Series in Computational Methods in Mechanics and Thermal Sciences, Hemisphere Publishing Corporation/ McGraw-Hill Book Company, Washington/New York, 1980.

[10] Y.S. Touloukian, P.E. Liley,Thermophysical Properties of Refrigerants, ASHRAE, New York, 1976.

[11] NIST, http://www.nist.gov/

Figure Captions

Fig.1 Physical model and coordinate system

Fig.2 Temperature profiles for $Ra = 4.87 \times 10^6$ **(a)** Frequency of 5 Hz with hot end upwards **(b)** Frequency of 10 Hz with hot end upwards **(c)** Frequency 5 Hz hot end downwards **(d)** Frequency 10 Hz hot end downwards

Fig.3 Temperature profiles for $Ra = 1.22 \times 10^6$ **(a)** Frequency 5 Hz hot end upwards **(b)** Frequency 10 Hz hot end upwards **(c)** Frequency 5 Hz hot end downwards **(d)** Frequency 10 Hz hot end downwards

Fig.4 Temperature and velocity variations for 5 Hz frequency 50 Pa amplitude during steady periodic conditions.**(a)** Temperature Variation **(b)** Velocity variation

Fig.5 Cross-section averaged temperature at different axial locations for $Ra = 1.22 \times 10^6$ with hot end up for 15 Hz frequency **(a)** 50Pa **(b)**500Pa

Fig.6 Cross-section averaged temperature at different axial locations for $Ra = 1.22 \times 10^6$ with hot end down for 15 Hz frequency **(a)** 50Pa hot end down **(b)** 500Pa hot end down

Fig.7 Axial temperature plot at 5 Hz with 50 Pa pressure amplitude. **(a)** $Ra = 4.87 \times 10^6$ and hot end up **(b)** $Ra = 4.87 \times 10^6$ and hot end down **(c)** $Ra = 1.22 \times 10^6$ and hot end up **(d)** $Ra = 1.22 \times 10^6$ and hot end down

Fig.8 Temperature and velocity plots for a $Ra = 1.22 \times 10^6$ and hot side up with constant and variable properties. **(a)** Temperature profile **(b)** Velocity profile

Fig.9 Heat transfer between gas and wall at different points with $Ra = 4.87 \times 10^6$ **(a)** Hot end up **(b)** Hot end down

Fig.10 Velocity plot for 15 Hz frequency and P_{a}=500 Pa. **(a)** Hot end up **(b)** Hot end down

Fig.11 Nusselt number plot for 15 Hz frequency and P_{a}=500 Pa. **(a)** Hot end up **(b)** Hot end down

Fig.12 Phase relationships between temperature and mass flow rate. **(a)** For $Ra = 4.87 \times 10^6$ and hot side up **(b)** For $Ra = 4.87 \times 10^6$ and hot side down **(c)** For $Ra = 1.22 \times 10^6$ and hot side up

List of Tables

Table 1: Details of parametric studies

Case no	Length (mm)	Diameter (mm)	Frequency (Hz)	Pressure amplitude (Pa)	Hot end temperature (K)	Cold end temperature (K)
Case: 1	100	8	5	50	300	100
Case: 2	100	8	5	500	300	100
Case: 3	100	8	10	50	300	100
Case: 4	100	8	15	50	300	100
Case: 5	100	8	5	500	300	100

Table 2: Results of the parametric studies for $Ra = 1.22 \times 10^6$ with hot side up

Case no	Pressure amplitude p_a (Pa)	Frequency (f) (Hz)	Time of operation (s)	Time average Nusselt Number (Nu_{av})
Case 1	50	5	501	3.64×10^{-2}
Case 2	500	5	501	4.22×10^{-2}
Case 3	50	10	501	8.00×10^{-2}
Case 4	50	15	501	7.28×10^{-2}
Case 5	500	15	501	2.73×10^{-2}

Table 3: Energy balance for different models for $Ra = 4.87 \times 10^6$ and hot side up

Case	Reynolds number (Re)	Time average gas enthalpy flow at $\frac{1}{2}H$ ($\dot{E}_{\mathrm{av}}$) (W)	Time average solid energy at $\frac{1}{2}H$ ($\dot{E}_{\mathrm{av}}$) (W)	Time average gas enthalpy flow at $\frac{3}{4}H$($\dot{E}_{\mathrm{av}}$) (W)	Time average solid energy at $\frac{3}{4}H$($\dot{E}_{\mathrm{av}}$) (W)
Case 1	140.48	1.74×10^5	2.66×10^{-2}	1.74×10^5	2.66×10^{-2}
Case 2	140.48	11.19×10^5	1.04×10^{-1}	11.19×10^5	1.04×10^{-1}
Case 3	280.96	1.15×10^5	1.8×10^{-2}	1.15×10^5	1.8×10^{-2}
Case 4	421.45	43.8×10^5	4.42×10^{-4}	43.8×10^5	4.42×10^{-4}
Case 5	421.45	68.79×10^5	8.09×10^{-4}	68.79×10^5	8.09×10^{-4}

Table 4: Energy balance for different models for $Ra = 1.22 \times 10^6$ and hot side down

Case	Reynolds number (Re)	Time average gas enthalpy flow at $\frac{1}{2}H$ ($\dot{E}_{\text{av}}$) (W)	Time average solid energy at $\frac{1}{2}H$ ($\dot{E}_{\text{av}}$) (W)	Time average gas enthalpy flow at $\frac{3}{4}H$($\dot{E}_{\text{av}}$) (W)	Time average solid energy at $\frac{3}{4}H$($\dot{E}_{\text{av}}$) (W)
Case 1	140.48	32.82×10^5	3.91×10^{-3}	32.82×10^5	3.91×10^{-3}
Case 2	140.48	32.78×10^5	3.22×10^{-2}	32.78×10^5	3.22×10^{-2}
Case 3	280.96	31.23×10^5	1.24×10^{-2}	31.23×10^5	1.24×10^{-2}
Case 4	421.45	8.46×10^6	2.31×10^{-4}	8.46×10^6	2.31×10^{-4}
Case 5	421.45	1.04×10^7	4.32×10^{-2}	1.04×10^7	4.32×10^{-2}

Figures

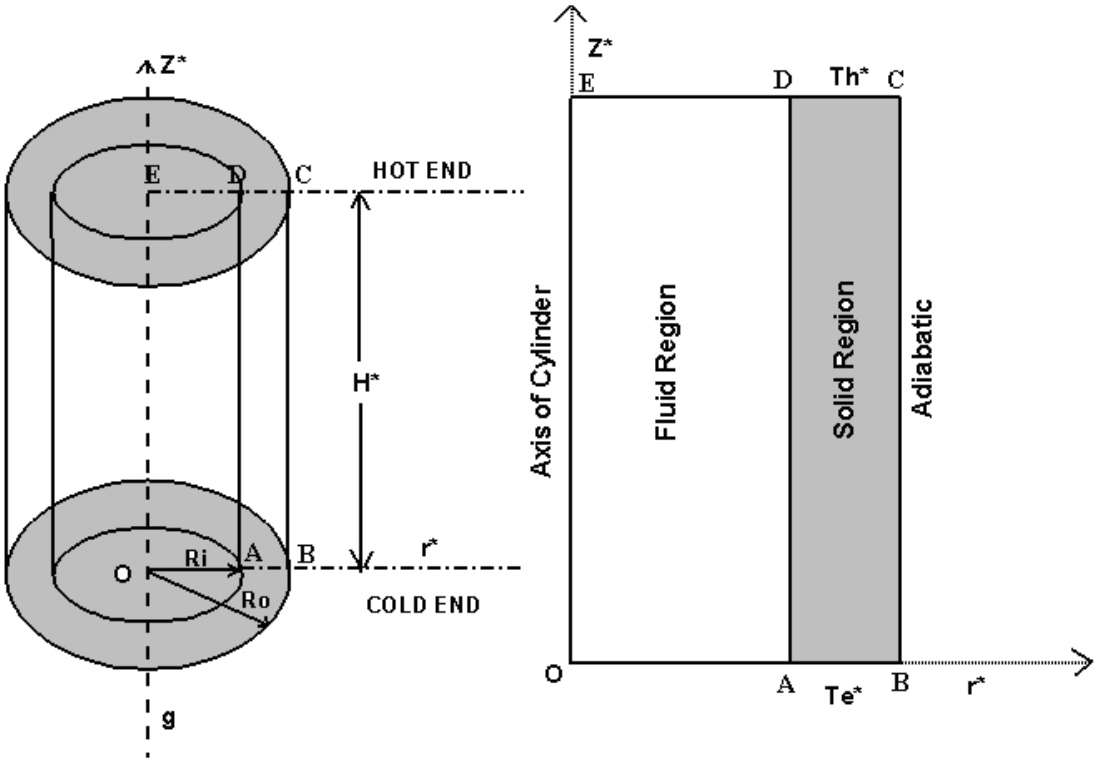

Figure 1:

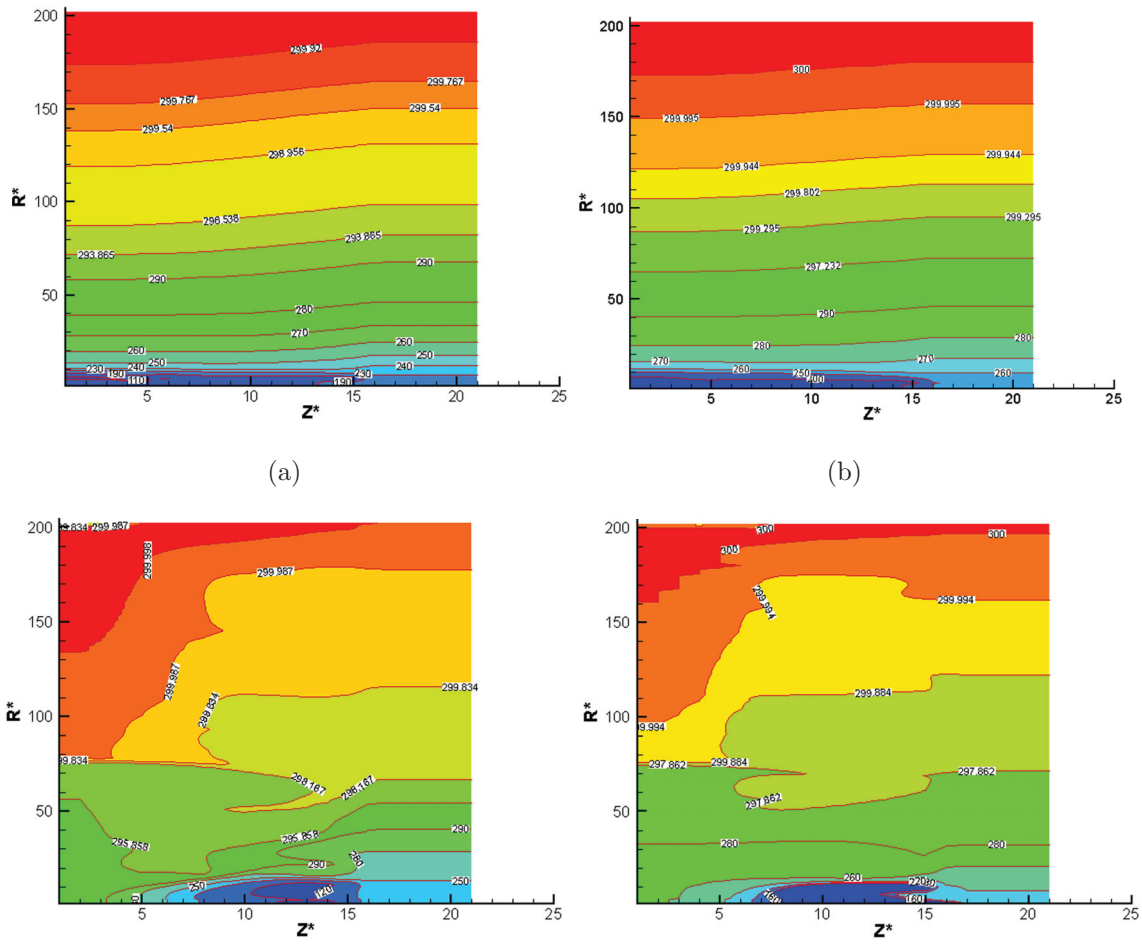

Figure 2:

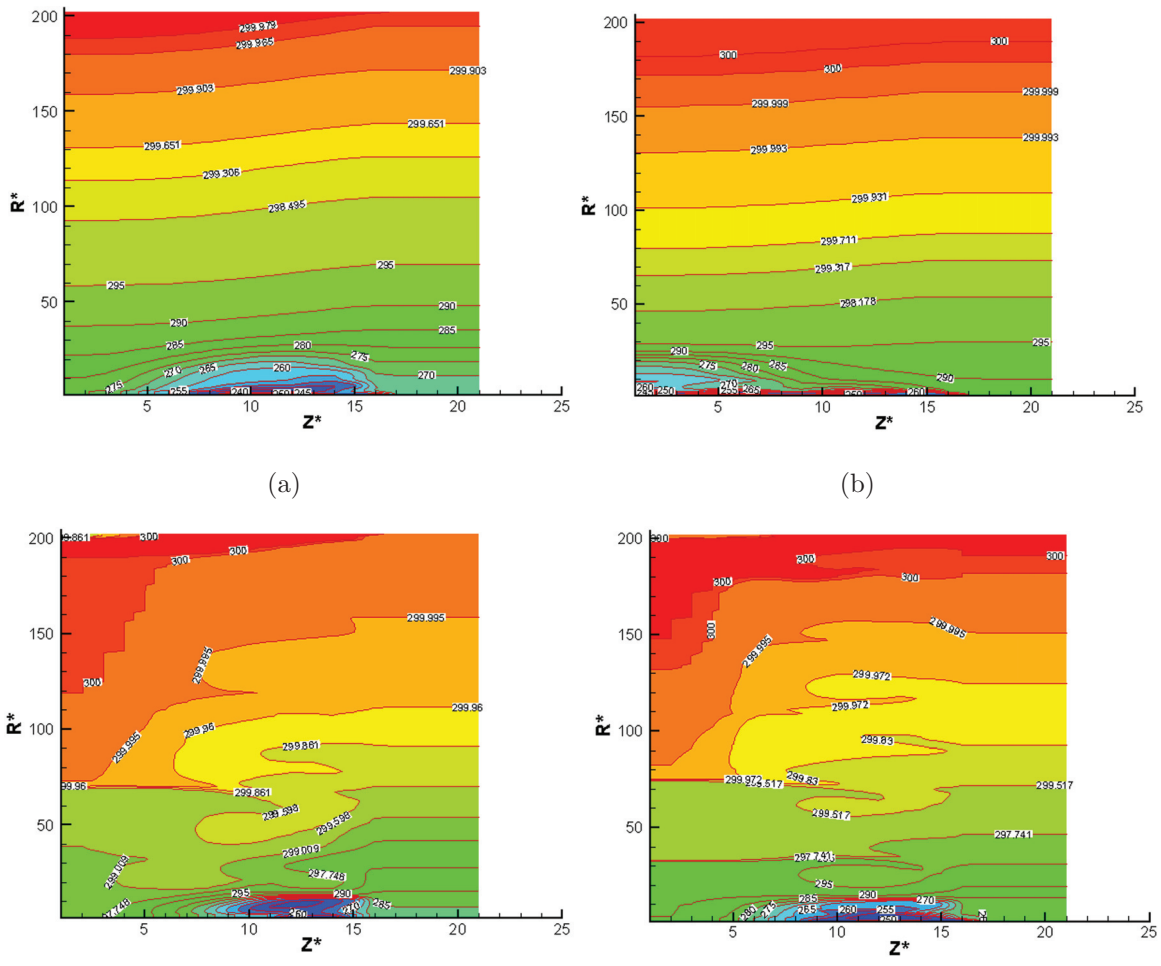

(a) (b)

(c) (d)

Figure 3:

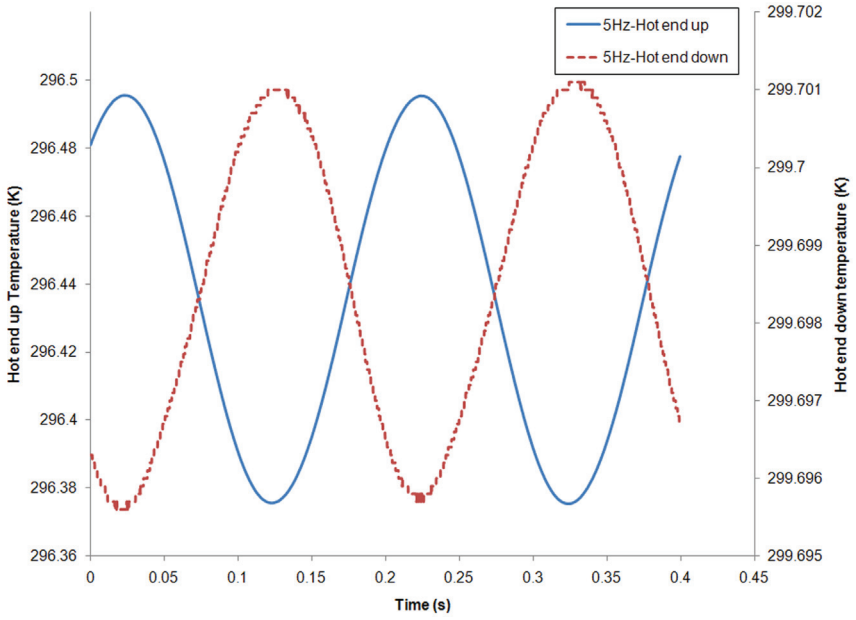
5Hz-Hot end up
5Hz-Hot end down
Hot end up Temperature (K)
Hot end down temperature (K)
Time (s)
296.5
296.48
296.46
296.44
296.42
296.4
296.38
296.36
299.702
299.701
299.7
299.699
299.698
299.697
299.696
299.695
0
0.05
0.1
0.15
0.2
0.25
0.3
0.35
0.4
0.45

(a)

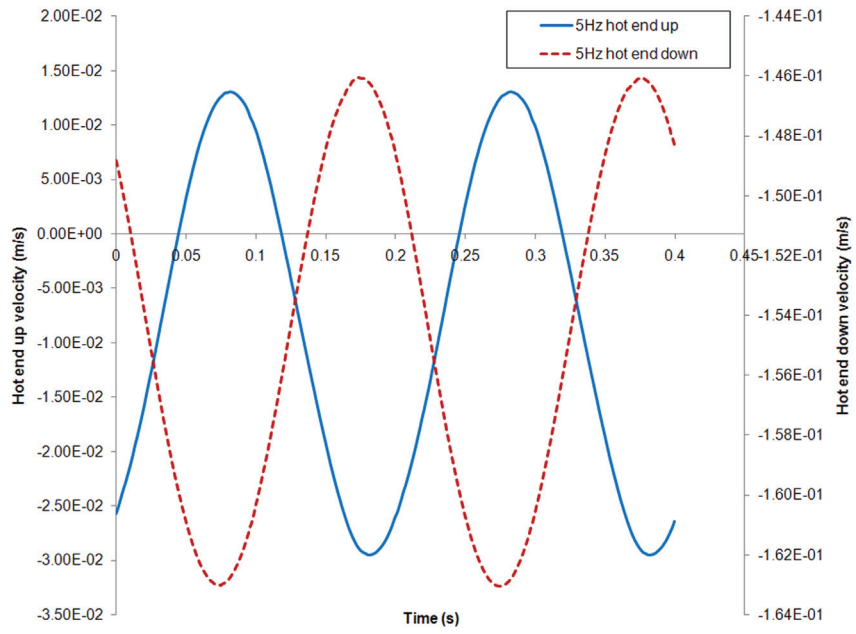
5Hz hot end up
5Hz hot end down
Hot end up velocity (m/s)
Hot end down velocity (m/s)
Time (s)
2.00E-02
1.50E-02
1.00E-02
5.00E-03
0.00E+00
-5.00E-03
-1.00E-02
-1.50E-02
-2.00E-02
-2.50E-02
-3.00E-02
-3.50E-02
-1.44E-01
-1.46E-01
-1.48E-01
-1.50E-01
-1.52E-01
-1.54E-01
-1.56E-01
-1.58E-01
-1.60E-01
-1.62E-01
-1.64E-01
0
0.05
0.1
0.15
0.2
0.25
0.3
0.35
0.4
0.45

(b)

Figure 4:

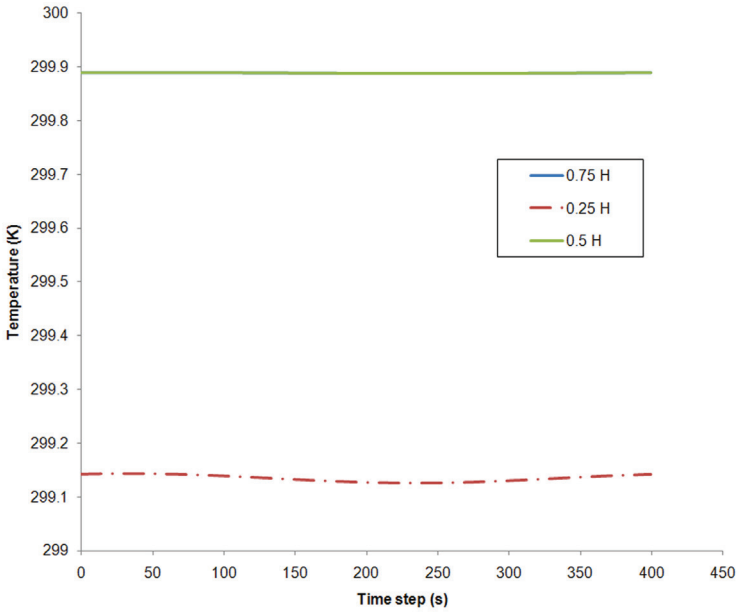
300
299.9
299.8
299.7
299.6
299.5
299.4
299.3
299.2
299.1
299
Temperature (K)
0
50
100
150
200
250
300
350
400
450
Time step (s)
0.75 H
0.25 H
0.5 H

(a)

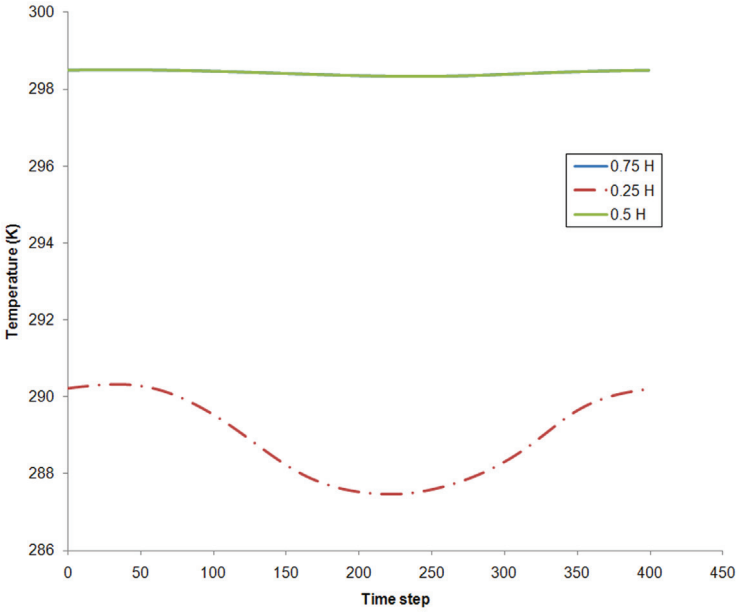
300
298
296
294
292
290
288
286
Temperature (K)
0
50
100
150
200
250
300
350
400
450
Time step
0.75 H
0.25 H
0.5 H

(b)

Figure 5:

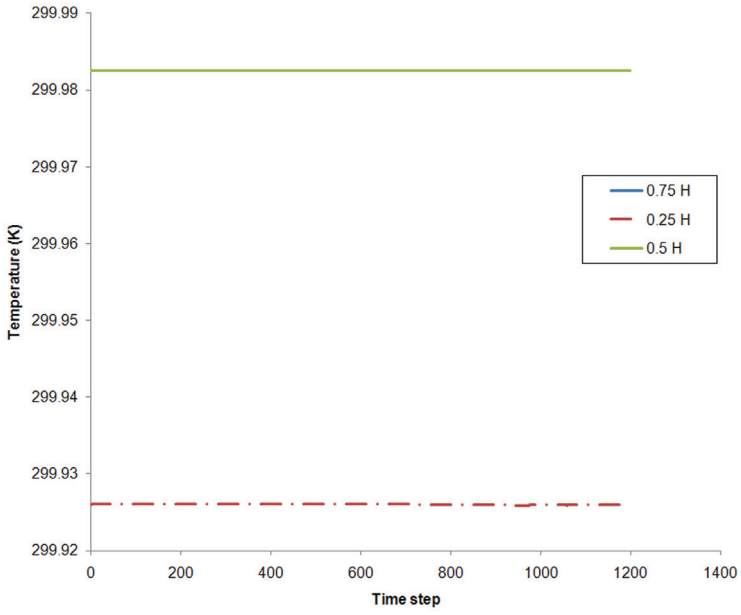
299.99
299.98
299.97
299.96
299.95
299.94
299.93
299.92
Temperature (K)
0
200
400
600
800
1000
1200
1400
Time step
0.75 H
0.25 H
0.5 H

(a)

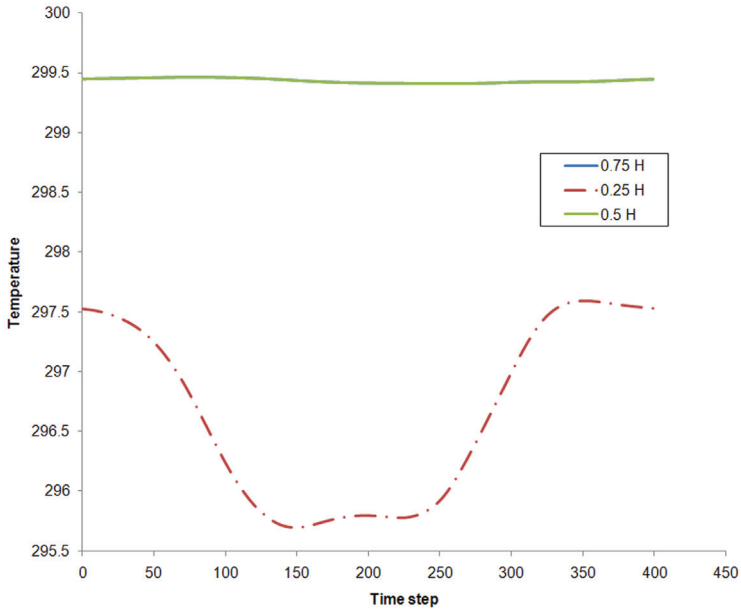
300
299.5
299
298.5
298
297.5
297
296.5
296
295.5
Temperature
0
50
100
150
200
250
300
350
400
450
Time step
0.75 H
0.25 H
0.5 H

(b)

Figure 6:

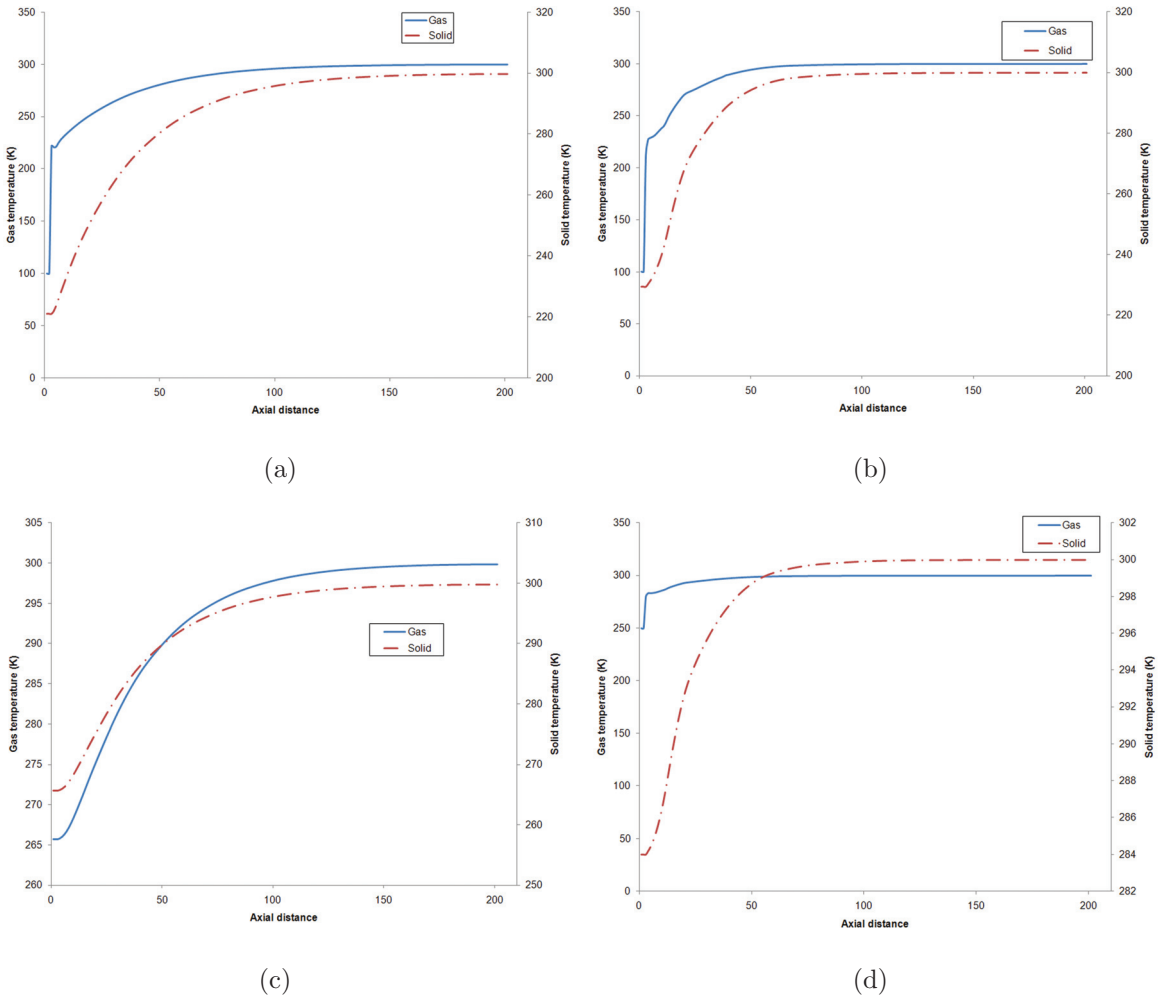
Gas
Solid
Gas temperature (K)
Solid temperature (K)
Axial distance
(a)
(b)
(c)
(d)

Figure 7:

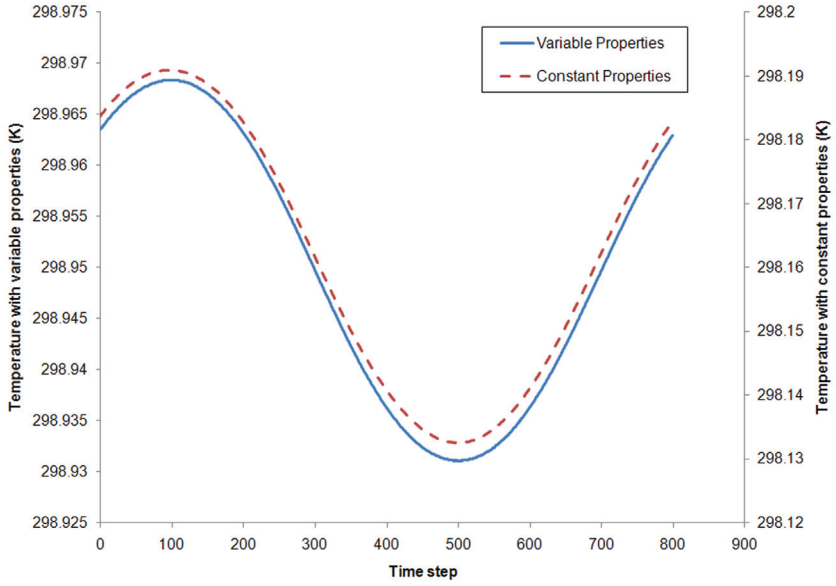
Variable Properties
Constant Properties
Temperature with variable properties (K)
Temperature with constant properties (K)
Time step
298.975
298.97
298.965
298.96
298.955
298.95
298.945
298.94
298.935
298.93
298.925
298.2
298.19
298.18
298.17
298.16
298.15
298.14
298.13
298.12
0
100
200
300
400
500
600
700
800
900

(a)

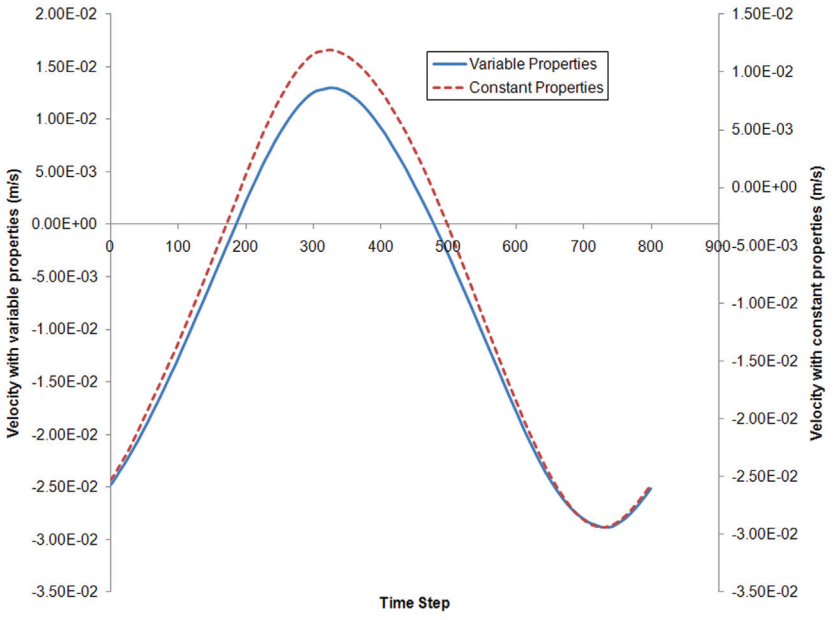
Variable Properties
Constant Properties
Velocity with variable properties (m/s)
Velocity with constant properties (m/s)
Time Step
2.00E-02
1.50E-02
1.00E-02
5.00E-03
0.00E+00
-5.00E-03
-1.00E-02
-1.50E-02
-2.00E-02
-2.50E-02
-3.00E-02
-3.50E-02
1.50E-02
1.00E-02
5.00E-03
0.00E+00
-5.00E-03
-1.00E-02
-1.50E-02
-2.00E-02
-2.50E-02
-3.00E-02
-3.50E-02
0
100
200
300
400
500
600
700
800
900

(b)

Figure 8:

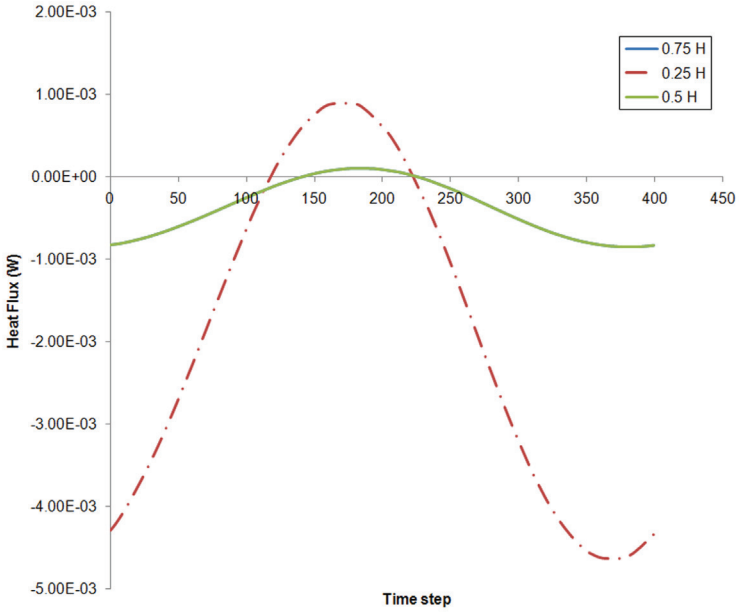
2.00E-03
1.00E-03
0.00E+00
-1.00E-03
-2.00E-03
-3.00E-03
-4.00E-03
-5.00E-03
0
50
100
150
200
250
300
350
400
450
0.75 H
0.25 H
0.5 H
Heat Flux (W)
Time step

(a)

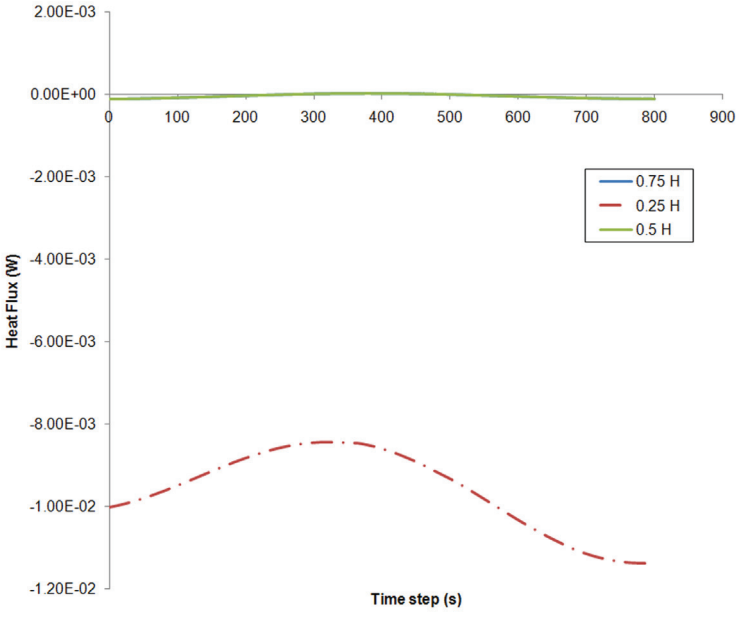
2.00E-03
0.00E+00
-2.00E-03
-4.00E-03
-6.00E-03
-8.00E-03
-1.00E-02
-1.20E-02
0
100
200
300
400
500
600
700
800
900
0.75 H
0.25 H
0.5 H
Heat Flux (W)
Time step (s)

(b)

Figure 9:

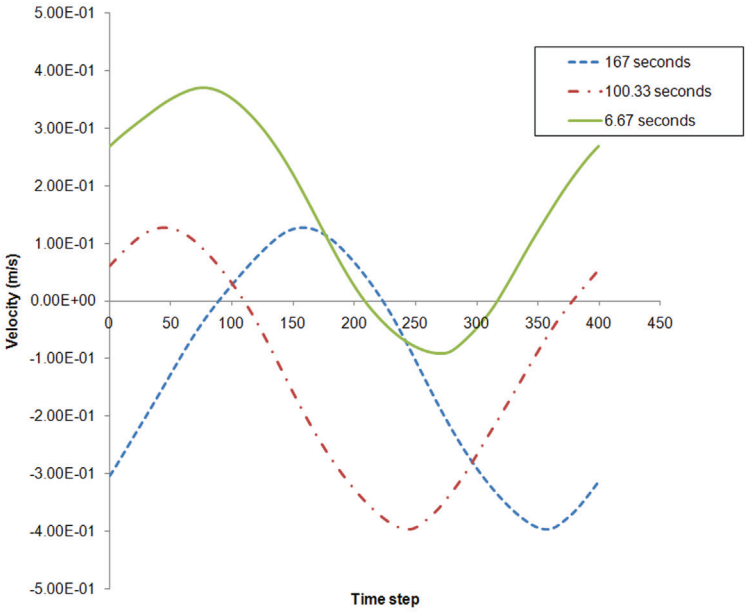
5.00E-01
4.00E-01
3.00E-01
2.00E-01
1.00E-01
0.00E+00
-1.00E-01
-2.00E-01
-3.00E-01
-4.00E-01
-5.00E-01
Velocity (m/s)
0
50
100
150
200
250
300
350
400
450
Time step
167 seconds
100.33 seconds
6.67 seconds

(a)

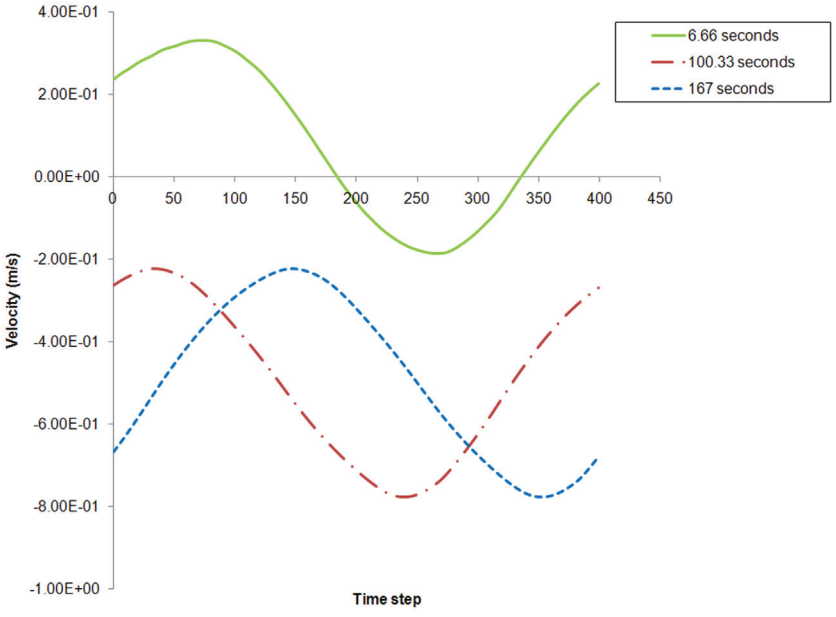
4.00E-01
2.00E-01
0.00E+00
-2.00E-01
-4.00E-01
-6.00E-01
-8.00E-01
-1.00E+00
Velocity (m/s)
0
50
100
150
200
250
300
350
400
450
Time step
6.66 seconds
100.33 seconds
167 seconds

(b)

Figure 10:

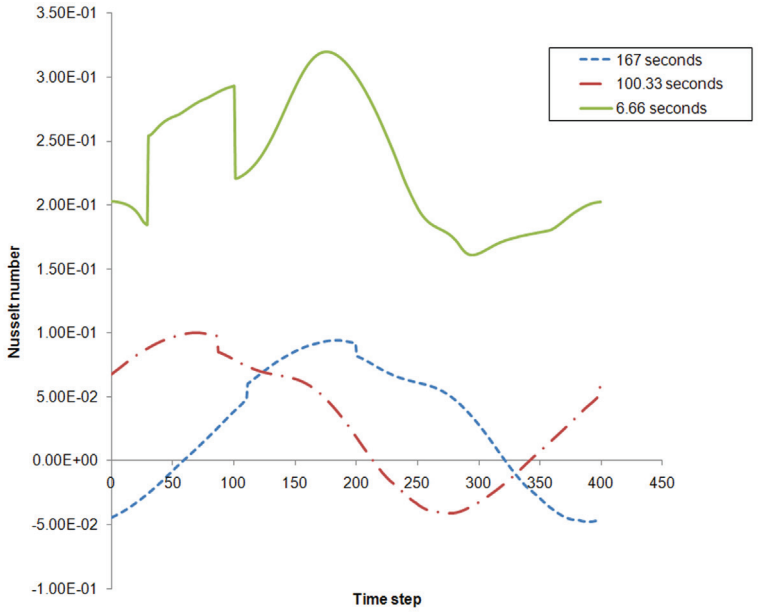
3.50E-01
3.00E-01
2.50E-01
2.00E-01
1.50E-01
1.00E-01
5.00E-02
0.00E+00
-5.00E-02
-1.00E-01
Nusselt number
0
50
100
150
200
250
300
350
400
450
Time step
167 seconds
100.33 seconds
6.66 seconds

(a)

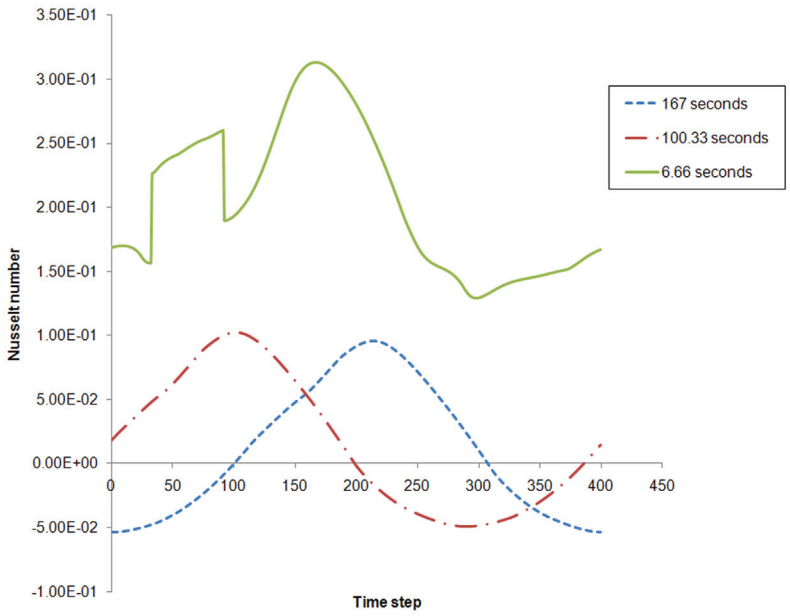
3.50E-01
3.00E-01
2.50E-01
2.00E-01
1.50E-01
1.00E-01
5.00E-02
0.00E+00
-5.00E-02
-1.00E-01
Nusselt number
0
50
100
150
200
250
300
350
400
450
Time step
167 seconds
100.33 seconds
6.66 seconds

(b)

Figure 11:

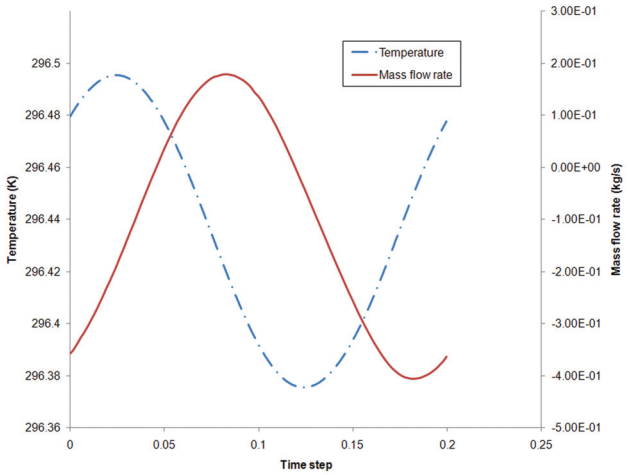

(a)

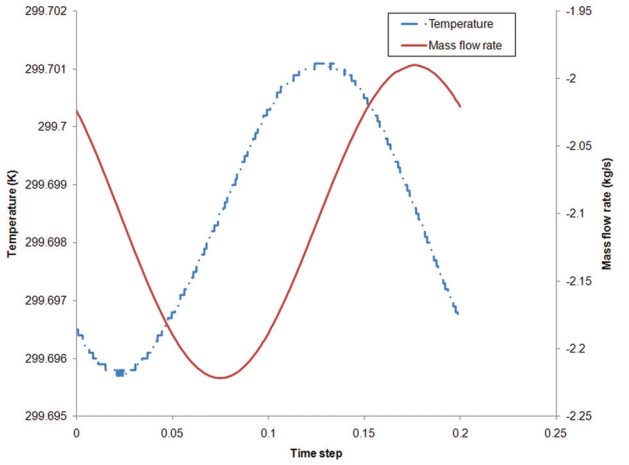

(b)

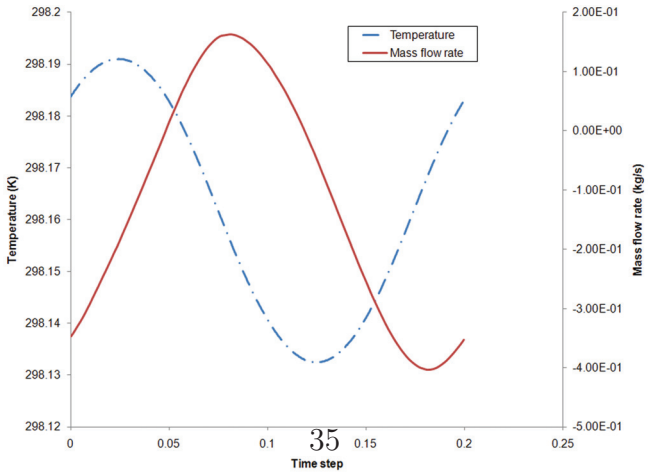

(c)

Figure 12: